



A numerical investigation of developing flow and heat transfer in a curved pipe

Flow and heat transfer in a curved pipe

M.R.H. Nobari and E. Amani
*Mechanical Engineering Department,
 Amirkabir University of Technology, Tehran, Iran*

847

Abstract

Purpose – This article aims to study numerically three dimensional developing incompressible flow and heat transfer in a fixed curved pipe.

Design/methodology/approach – A projection algorithm based on the second order finite difference method is used for discretizing governing equations written in the toroidal coordinate system.

Findings – The effects of curvature and governing non-dimensional parameters consisting of Reynolds, Prandtl, and Dean numbers on the flow field, entrance length, and heat transfer are studied in detail. The numerical results indicate that the entrance length depends only on the Reynolds number for the curvature ratios greater than 1/7 and therefore, Dean number is not a pertinent parameter in this range.

Research limitations/implications – For heat transfer analysis, two different thermal boundary conditions, i.e. constant wall temperature and constant heat flux at the wall are implemented. The results are calculated for the Dean numbers in the range of 76-522 and for the two prandtl numbers of 0.5 and 1.

Practical implications – The results can be used in designing heat exchangers, piping systems, and cooling of gas turbine blades.

Originality/value – The numerical results obtained here concentrate on the detailed investigation of flow and temperature field at the entrance region by a quantitative analysis of hydrodynamic and thermal entrance length. The effects of different thermal boundary conditions and different inlet profiles on the flow and temperature fields are studied in the circular curved pipe for the first time.

Keywords Flow, Finite difference methods, Pipes, Heat transfer, Curve fitting, Fluid dynamics

Paper type Research paper

Received 11 May 2007
 Revised 1 May 2009
 Accepted 1 May 2009

Nomenclature

Latin symbols

a	= Pipe radius	p	= Pressure
C_f	= Friction factor	Pr	= Prandtl number
C_p	= Specific heat at constant pressure	q_w	= Heat flux at the wall
d	= Pipe diameter	\vec{r}	= Position vector
Ec	= Eckert number	r	= Radial direction
h	= Convection heat transfer coefficient	R	= Curvature
k	= Thermal conductivity	Re	= Reynolds number
K_{LC} (or De)	= Dean number	t	= Time
Nu	= Nusselt number	T	= Temperature
		u	= Radial velocity
		\vec{V}	= Velocity vector



v = Circumferential velocity
 w_m = Mean axial velocity
 w = Axial velocity

Subscripts

0 = at ($r = 0, \theta = 0$)
 b = Bulk property
 c = Curved pipe
 fd = Fully developed condition
 h = Hydrodynamic
 m = Cross sectional averaged value
 s = Straight pipe, surface
 t = Total value, thermal
 w = Pipe wall

Greek symbols

δ = Curvature ratio
 θ = Axial direction
 μ = Viscosity
 τ = Stress
 ρ = Density
 Φ = Circumferential direction

Superscripts

' = Dimensional quantity

1. Introduction

Flow and heat transfer in a curved pipe is one of the most attractive research fields of thermofluid mechanics. It arises in many engineering problems such as heat exchangers, bends in piping systems, cooling of gas turbine blades and in bio-fluid mechanics, especially blood flow in the aorta.

Owing to the presence of a secondary motion caused by centrifugal effects, the location of the maximum axial velocity moves towards the outer wall of a curved pipe, as it was first discovered by Williams *et al.* (1902). Dean (1927, 1928), for the first time, showed that the flow in slightly curved pipes depends primarily on a single non-dimensional parameter called Dean number, De . Centrifugal forces give rise to a secondary flow that consists of a pair of counter-rotating cells, called Dean cells. For higher Dean numbers, centrifugal instability appears close to the outer wall, generating additional pair of counter-rotating vortices known as Dean vortices. Dean cells are present even at the lowest Dean numbers due to the imbalance between centrifugal and viscous forces. More detailed studies of the hydrodynamics of Dean flow have been reported by Berger *et al.* (1983), Bara *et al.* (1992), and Le Guer *et al.* (2001).

Austin (1971), Patankar *et al.* (1974), and Humphrey (1977) carried out finite difference calculations of the flow development in a curved pipe beginning with Poiseuille flow at the inlet. Soh and Berger (1984) investigated the development of entry flow in a curved pipe and observed secondary flow separation near the inner wall in the developing region resulting in two-step plateau-like axial velocity profiles at high Dean numbers.

The secondary flow improves the global heat transfer. For instance, the inner Nusselt number of a helical coil is higher than that of a straight tube (Shah and Joshi, 1987). Acharya *et al.* (1993) showed that in coiled tubes periferally averaged Nusselt number undergoes spatial oscillations before reaching an axially invariant fully developed value.

Ishigaki (1996) examined the flow structure and friction factor numerically for fixed and rotating curved pipes with a small curvature and presented semi-empirical formulas for the friction factor and Nusselt number in fully developed region (Ishigaki, 1994, 1996).

Zheng *et al.* (2000) studied combined forced convection, buoyancy, and thermal radiation in the entrance region of helical pipes and found that the buoyancy has more effects in temperature field than it has in velocity field. Kumar and Nigam (2005) simulated entrance flow filed in a curved pipe numerically with a first order finite-volume method.

The analogy between the flows through stationary curved ducts and orthogonally rotating straight ducts have been qualitatively performed for a circular cross section by several authors (Trefethen, 1957; Ito and Nanbu, 1971). In the case of rectangular ducts, Papa *et al.* (2002) reported that for high Reynolds and rotation numbers, flow patterns in rectangular ducts can break into two or more pair of vortices; Lee and Baek (2006) showed that for the flow field satisfied the “asymptotic invariance property”, there were strong quantitative similarities between the two flows. Based on these similarities, it is possible to predict the flow characteristics in rotating ducts by considering the flow in stationary curved ducts, and vice versa.

In this article, developing fluid flow and heat transfer are numerically investigated using a projection method based on the second order finite difference discretization of the governing equations written in the toroidal coordinate system. Heat transfer is considered at two different boundary conditions including the constant wall temperature and constant heat flux at the wall. Although several similar studies have been carried out previously, there is no precise quantitative analysis of the hydrodynamic and thermal entrance lengths for the flow in the curved pipes at different inlet conditions. Therefore, the numerical results obtained here concentrate on the detailed investigation of the flow and temperature fields in the entrance region of the curved pipes to precisely analyze the hydrodynamic and thermal entrance lengths at different inlet conditions. The effects of Dean number on the flow field, entrance length, secondary flow, and heat transfer are studied in detail. Here, loose coil approximation ($\delta < 1/16$) is not used to simplify the equations (Nobari and Gharali, 2006), and the results for high curvature values are compared with the loose one. Semi-empirical available data (Ishigaki, 1994, 1996) for the case of loose curvature are taken into account for validation of current results.

2. Mathematical formulation

2.1 Governing equations

Using the characteristic values consisting of density, ρ' , viscosity, μ' , pipe radius, a' , inlet axial velocity at the center, W'_0 , inlet temperature at the center, T'_0 , the non-dimensional variables are defined as

$$\begin{aligned} \vec{r} &= \frac{\vec{r}'}{a'}, & \vec{V} &= \frac{\vec{V}'}{W'_0}, & p &= \frac{p'}{\rho' W'^2_0} \\ \tau &= \frac{\tau' a'}{\mu' W'_0}, & T &= \frac{T' - T'_0}{T^{*'} - T'_0} \end{aligned} \quad (1)$$

where primed quantities are dimensional and $T^{*'}$ is a characteristic temperature which will be defined based on the thermal boundary conditions at the wall. Taking into account the characteristic parameters mentioned above the following non-dimensional parameters can be defined.

$$Re = \frac{\rho' a' W'_0}{\mu'}, \quad Pr = \frac{\mu' c'_p}{k'}, \quad Ec = \frac{W'^2_0}{c'_p (T^{*' } - T'_0)} \quad (2)$$

where $T^{*'}$ is considered as

$$\begin{aligned} T^{*' } &= T'_s; & \text{for constant wall temperature} \\ T^{*' } &= T'_0 + \frac{q'_w a'}{k'}; & \text{for constant wall heat flux} \end{aligned} \quad (3)$$

By this definition for the non-dimensional temperature, T , the energy equation will be identical for two different thermal boundary conditions at the wall.

For incompressible viscous flow neglecting gravity, the continuity, momentum, and energy equations in non-dimensional forms using the toroidal coordinates (r, ϕ, θ) shown in Figure 1 may be written as (Berger *et al.*, 1983)

continuity

$$\frac{\partial}{\partial r}(rBu) + \frac{\partial}{\partial \phi}(Bv) + \frac{\partial}{\partial \theta}(\delta rw) = 0 \quad (4)$$

radial momentum

$$\begin{aligned} & \frac{\partial u}{\partial t} + \frac{1}{rB} \left[\frac{\partial}{\partial r}(rBu^2) + \frac{\partial}{\partial \phi}(Buv) + \frac{\partial}{\partial \theta}(\delta ruw) - Bv^2 - \delta rw^2 \cos \phi \right] \\ & = -\frac{\partial p}{\partial r} + \frac{1}{Re} \left\{ \frac{1}{rB} \left[\frac{\partial}{\partial r} \left(rB \frac{\partial u}{\partial r} \right) + \frac{\partial}{\partial \phi} \left(\frac{B}{r} \frac{\partial u}{\partial \phi} \right) + \frac{\partial}{\partial \theta} \left(\frac{\delta^2 r}{B} \frac{\partial u}{\partial \theta} \right) \right] \right. \\ & \left. - \frac{1}{r^2} \left(2 \frac{\partial v}{\partial \phi} + u \right) + \frac{\delta v \sin \phi}{rB} + \frac{\delta^2 \cos \phi}{B^2} \left(v \sin \phi - u \cos \phi - 2 \frac{\partial w}{\partial \theta} \right) \right\} \end{aligned} \quad (5)$$

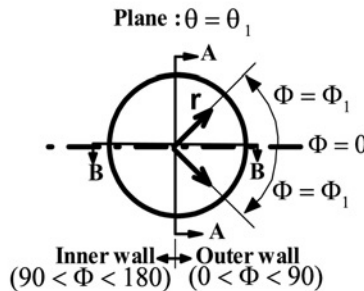
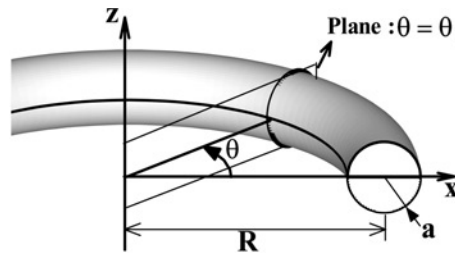


Figure 1.
(top) Curved pipe geometry in toroidal coordinate system
(bottom) different regions of a cross section

Notes: Left semicircle is the inner wall and right one is the outer wall, section B-B is the plane of symmetry and section A-A is the plane perpendicular to the plane of symmetry. The angle Φ increases counterclockwise in upper half and clockwise in lower half of the tube. These conventions are held in other figures

circumferential momentum

Flow and heat
transfer in a
curved pipe

$$\begin{aligned} & \frac{\partial v}{\partial t} + \frac{1}{rB} \left[\frac{\partial}{\partial r} (rBuv) + \frac{\partial}{\partial \phi} (Bv^2) + \frac{\partial}{\partial \theta} (\delta r v w) + Buv + \delta r w^2 \sin \phi \right] \\ &= -\frac{\partial p}{\partial \phi} + \frac{1}{Re} \left\{ \frac{1}{rB} \left[\frac{\partial}{\partial r} \left(rB \frac{\partial v}{\partial r} \right) + \frac{\partial}{\partial \phi} \left(\frac{B}{r} \frac{\partial v}{\partial \phi} \right) + \frac{\partial}{\partial \theta} \left(\frac{\delta^2 r}{B} \frac{\partial v}{\partial \theta} \right) \right] \right. \\ & \left. + \frac{1}{r^2} \left(2 \frac{\partial u}{\partial \phi} - v \right) - \frac{\delta u \sin \phi}{rB} - \frac{\delta^2 \sin \phi}{B^2} \left(v \sin \phi - u \cos \phi - 2 \frac{\partial w}{\partial \theta} \right) \right\} \end{aligned} \quad (6)$$

851

axial momentum

$$\begin{aligned} & \frac{\partial w}{\partial t} + \frac{1}{rB} \left[\frac{\partial}{\partial r} (rBuw) + \frac{\partial}{\partial \phi} (Bvw) + \frac{\partial}{\partial \theta} (\delta r w^2) + \delta r w (u \cos \phi - v \sin \phi) \right] \\ &= -\frac{\delta \partial p}{B \partial \theta} + \frac{1}{Re} \left\{ \frac{1}{rB} \left[\frac{\partial}{\partial r} \left(rB \frac{\partial w}{\partial r} \right) + \frac{\partial}{\partial \phi} \left(\frac{B}{r} \frac{\partial w}{\partial \phi} \right) + \frac{\partial}{\partial \theta} \left(\frac{\delta^2 r}{B} \frac{\partial w}{\partial \theta} \right) \right] \right. \\ & \left. + \frac{2\delta^2}{B^2} \left(\frac{\partial u}{\partial \theta} \cos \phi - \frac{\partial v}{\partial \theta} \sin \phi - \frac{w}{2} \right) \right\} \end{aligned} \quad (7)$$

energy

$$\begin{aligned} & \frac{\partial T}{\partial t} + \frac{1}{rB} \left[\frac{\partial}{\partial r} (rBuT) + \frac{\partial}{\partial \phi} (BvT) + \frac{\partial}{\partial \theta} (\delta r w T) \right] \\ &= Ec \left\{ \frac{\partial p}{\partial t} + \frac{1}{rB} \left[\frac{\partial}{\partial r} (rBup) + \frac{\partial}{\partial \phi} (Bvp) + \frac{\partial}{\partial \theta} (\delta r w p) \right] \right\} \\ &+ \frac{1}{RePr} \left\{ \frac{1}{rB} \left[\frac{\partial}{\partial r} \left(rB \frac{\partial T}{\partial r} \right) + \frac{\partial}{\partial \phi} \left(\frac{B}{r} \frac{\partial T}{\partial \phi} \right) + \frac{\partial}{\partial \theta} \left(\frac{\delta^2 r}{B} \frac{\partial T}{\partial \theta} \right) \right] \right\} \end{aligned} \quad (8)$$

where

$$\delta = \frac{a'}{R}, \quad B = 1 + \delta r \cos \phi \quad (9)$$

and u, v, w are the velocity components in r, ϕ and θ directions, respectively.

Other non-dimensional flow quantities and parameters are defined as

$$\begin{aligned} \tau_{rr} &= 2 \frac{\partial u}{\partial r} \\ \tau_{\phi\phi} &= \frac{2}{r} \left(\frac{\partial v}{\partial \phi} + u \right) \\ \tau_{\theta\theta} &= \frac{2\delta}{B} \left(\frac{\partial w}{\partial \theta} + u \cos \phi - v \sin \phi \right) \\ \tau_{r\phi} = \tau_{\phi r} &= \frac{\partial v}{\partial r} + \frac{1}{r} \frac{\partial u}{\partial \phi} - \frac{v}{r} \\ \tau_{\phi\theta} = \tau_{\theta\phi} &= \frac{1}{r} \frac{\partial w}{\partial \phi} + \frac{\delta}{B} \frac{\partial v}{\partial \theta} + \frac{\delta w \sin \phi}{B} \\ \tau_{r\theta} = \tau_{\theta r} &= \frac{\delta}{B} \frac{\partial u}{\partial \theta} + \frac{\partial w}{\partial r} - \frac{\delta w \cos \phi}{B} \end{aligned} \quad (10)$$

$$\tau_w = \sqrt{\tau_{r\phi}^2 + \tau_{r\theta}^2} \quad (11)$$

$$C_f = \frac{\tau_w/w_m^2}{\frac{1}{2}Re}, C_{f,m} = \frac{1}{2\pi} \int_0^{2\pi} C_f d\phi, C_{f,t} = \frac{1}{\theta_{fd}} \int_0^{\theta_{fd}} C_{f,m} d\theta \quad (12)$$

where w_m is the non-dimensional mean axial velocity; C_f , local friction factor, $C_{f,m}$, cross sectional average friction factor; and $C_{f,t}$, average friction factor for a curved pipe (overall entrance region).

With the bulk fluid temperature, T'_b ,

$$T'_b = \frac{\int_A w' T' dA}{\int_A w' dA} \quad (13)$$

local convection heat transfer coefficient can be obtained as

$$h' = \frac{q'_w}{|T'_s - T'_b|} \quad (14)$$

At the constant wall temperature case using Equations (3) and (14), local Nusselt number, $Nu = \frac{h'd}{k}$, and its cross sectional average are obtained as

$$Nu = \frac{\left(\frac{\partial T}{\partial r}\right)_{r=1}}{|1 - T_b|}, \quad Nu_m = \frac{1}{2\pi} \int_0^{2\pi} Nu d\phi \quad (15)$$

For constant heat flux case, cross sectional average convection heat transfer coefficient is defined by substituting T'_s with the mean surface temperature at each cross section, $T'_{s,m}$, through Equation (14). Therefore, using Equation (3), cross sectional average Nusselt number for constant heat flux at the wall is determined as

$$Nu_m = \frac{1}{|T_{s,m} - T_b|} \quad (16)$$

Overall average Nusselt number, Nu_t , in the entrance region can be determined as

$$Nu_t = \frac{1}{\theta_{fd}} \int_0^{\theta_{fd}} Nu_m d\theta \quad (17)$$

Another important non-dimensional parameter is the Dean number, De or K_{LC} , which is defined as follows (Lee and Baek, 2002; Nobari and Gharali, 2006)

$$De = K_{LC} = Re_m \sqrt{2\delta} \quad (18)$$

where $Re_m = \frac{\rho' d' w'_m}{\mu'} = 2w_m \times Re$, is the conventional Reynolds number based on bulk velocity and pipe diameter.

2.2 Boundary conditions

Here, the inlet hydrodynamic boundary condition is considered to be the fully developed velocity profile obtained from the analytical solution of fluid flow in a straight pipe (Bejan, 1984). Therefore, it can be written as

$$u(r, \phi, 0) = v(r, \phi, 0) = 0, \quad w(r, \phi, 0) = 1 - r^2 \quad (19)$$

For the inlet temperature, two different boundary conditions are taken into account including uniform temperature (I.B.1) and fully developed temperature concerning the thermal boundary conditions at the wall of the straight pipe (I.B.2). Therefore, two different cases are studied at each thermal boundary at the wall.

In the case of constant heat flux at the wall, the inlet temperatures are considered as

$$T(r, \phi, 0) = 0; \quad (I.B.1) \quad (20)$$

$$T(r, \phi, 0) = r^2 - \frac{r^4}{4}; \quad (I.B.2) \quad (21)$$

In the case of constant wall temperature the inlet temperatures are defined as

$$T(r, \phi, 0) = 0; \quad (I.B.1) \quad (22)$$

$$\frac{d^2 T}{dr^2} + \frac{1}{r} \frac{dT}{dr} + 4Nu(1 - r^2)(T - 1) = 0, \quad (23)$$

$$T(r = 0) = 0, \quad T(r = 1) = 1; \quad (I.B.2)$$

The above equation is solved numerically to obtain the concerning fully developed temperature for the straight pipe, which is used as the inlet temperature of the curved pipe.

No-slip boundary conditions are applied at the wall for velocities, and two thermal boundaries consisting of constant wall temperature and constant heat flux at the wall are used.

$$u(1, \phi, \theta) = v(1, \phi, \theta) = w(1, \phi, \theta) = 0,$$

$$T(1, \phi, \theta) = 1 \quad ; \text{ constant wall temperature}$$

$$\frac{\partial T}{\partial r} = 1 \quad \text{at} \quad r = 1 \quad ; \text{ constant wall heat flux} \quad (24)$$

Assuming fully developed conditions at the outlet of the curved pipe, the following Neumann boundary conditions are implemented:

$$\frac{\partial u}{\partial \theta} = \frac{\partial v}{\partial \theta} = \frac{\partial w}{\partial \theta} = 0 \quad \text{at} \quad \theta = \theta_{fd,h}$$

$$\frac{\partial}{\partial \theta} \left(\frac{T - T_s}{T_b - T_s} \right) = 0 \quad \text{at} \quad \theta = \theta_{fd,t} \quad (25)$$

This general form of fully developed thermal boundary condition can be made simpler in each case of thermal boundary conditions at the wall (Nobari and Gharali, 2006).

Since the flow field in a curved pipe is symmetrical relative to the horizontal mid-plane, it is enough to solve the governing equations in upper or lower half of the curved

pipe. Therefore, the boundary conditions at the plane of symmetry are

$$\frac{\partial u}{\partial \phi} = \frac{\partial w}{\partial \phi} = \frac{\partial T}{\partial \phi} = v = 0 \quad \text{at} \quad \phi = 0, \pi \quad (26)$$

3. Numerical method

An O-type structured orthogonal grid system, shown in Figure 2(a), has been generated to solve the governing equations in the toroidal coordinate system employing projection method which is based on the second order discretization in space and first order forward in time.

The projection algorithm introduced by Chorin (1968) and independently by Temam (1978) is one of the most powerful numerical tools used in solving incompressible Navier-Stokes equations at moderate Reynolds numbers. It has been employed successfully for convection problems by finite difference (Lee and Baek, 2002) and finite element (Nonino and Comini, 2002; Comini *et al.*, 2004) methods. Using the projection method, the Navier-Stokes equation is split into two simpler equations which are linked by satisfying continuity to obtain a Poisson equation for the pressure field. Briefly, the algorithm is explained at the following.

Employing a provisional velocity (\vec{V}^*), the first step of the projection method is written as

$$\frac{\vec{V}^* - \vec{V}^n}{\Delta t} + [(\vec{V} \cdot \nabla) \vec{V}]^n = \frac{1}{Re} \nabla^2 \vec{V}^n \quad (27)$$

which is the momentum equation without the pressure gradient term. Then at the second step, the provisional velocity is corrected by considering the following equations:

$$\frac{\vec{V}^{n+1} - \vec{V}^*}{\Delta t} + \nabla p^{n+1} = 0 \quad (28)$$

Taking the divergence of above equation and satisfying continuity at new time step ($\nabla \cdot \vec{V}^{n+1} = 0$), the Poisson equation for the pressure is obtained as

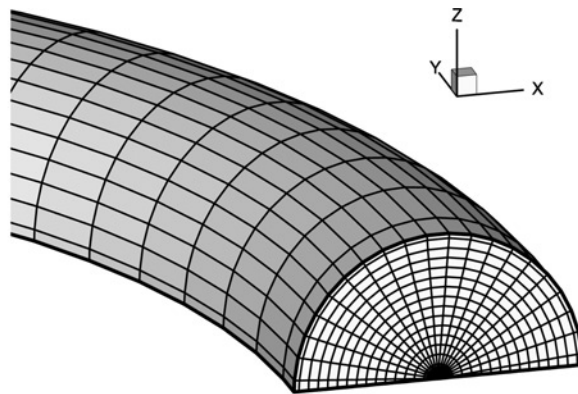
$$\nabla^2 p^{n+1} = \frac{1}{\Delta t} \nabla \cdot \vec{V}^* \quad (29)$$

After computing \vec{V}^* by Equation (27), p^{n+1} is obtained solving the Poisson equation (Equation (29)) via an iterative method. Finally, velocity \vec{V}^{n+1} is corrected using Equation (28) and algorithm proceeds to next time step. Since an explicit method is used to solve the unsteady full Navier-Stokes equations, through von Neumann stability method (Anderson, 1995) the following stability conditions need to be satisfied for each cell

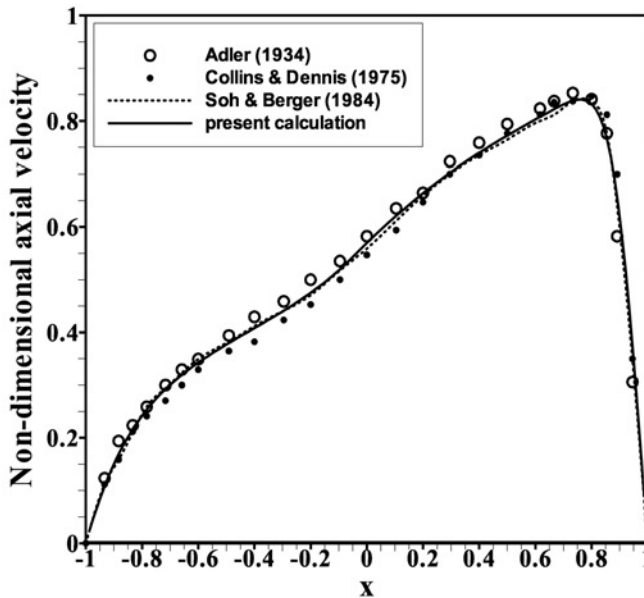
$$\frac{\Delta t_{cell}}{Re \Delta h_{min}^2} \leq \frac{1}{6}, \quad \Delta t_{cell} Re V_{max}^2 \left(\frac{h_{min}}{h_{max}} \right)^2 \leq 1 \quad (30)$$

where, h_{min} and h_{max} are

$$h_{min} = \min(\Delta r, r \Delta \Phi, \frac{B}{\delta} \Delta \theta), \quad h_{max} = \max(\Delta r, r \Delta \Phi, \frac{B}{\delta} \Delta \theta)$$



(a)



(b)

Notes: The results: measured by Adler (1934) for $Dean = 526$, computed by Collins and Dennis (1975) for $Dean = 522.5$, computed by Soh and Berger (1984) for $Dean = 522.4$ ($\delta = 1/20$, $Re = 1652$)

Figure 2.
 (a) Structured grid topology and (b) comparison of fully developed axial velocity on the plane of symmetry (section B-B) for $Dean = 522.4$ ($\delta = 1/20$, $Re = 1,652$)

The time step, Δt used in the numerical calculation can be at most equal to the smallest cell time step. The choice of grid resolution depends on the Dean and Reynolds numbers, consequently, the resolutions considered here vary from 30×38 to 40×40 in $r \times \phi$ and 23 to 75 in θ direction. For this mesh sizes, to satisfy stability conditions, time step sizes are at the order of 10^{-3} to 10^{-4} .

It should be declared that the maximum error of the residuals in all runs is set to be of the order of 10^{-8} .

Validation of results has been done by a comparison with previous works as shown in Figure 2(b). To test the conservative property of the developed code, the grid independency test has been successfully carried out for different grid sizes, which is shown in Figure 3.

4. Results and discussion

To study developing flow and heat transfer in a curved pipe, direct numerical simulation is carried out for Dean numbers at the range of 76-522 and the Reynolds numbers from 242 to

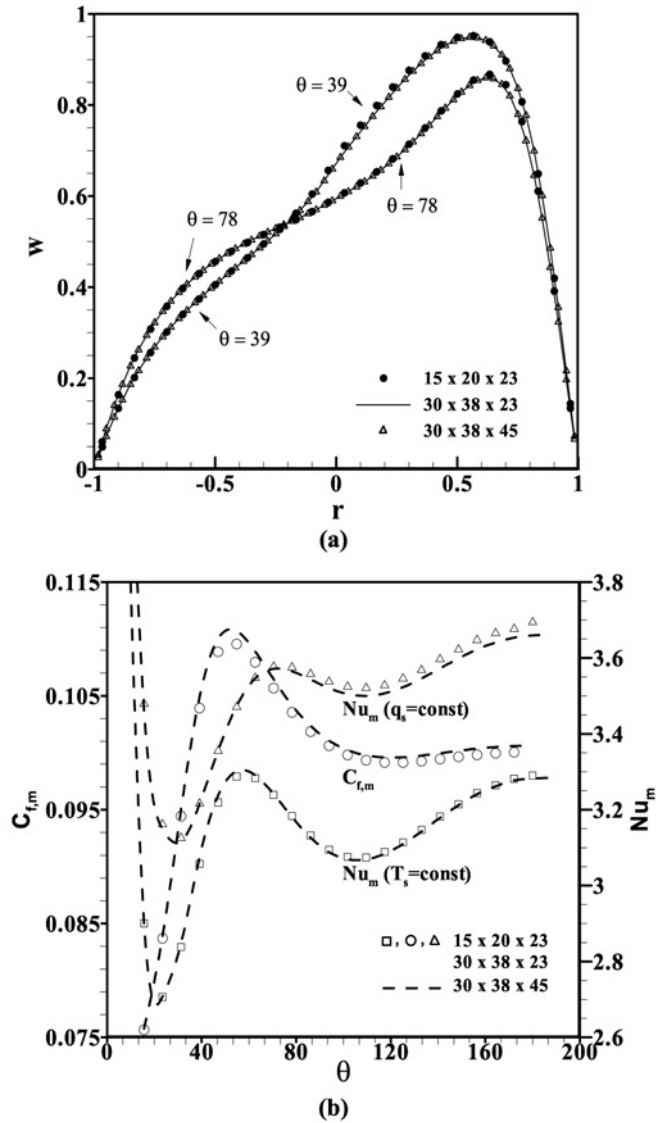
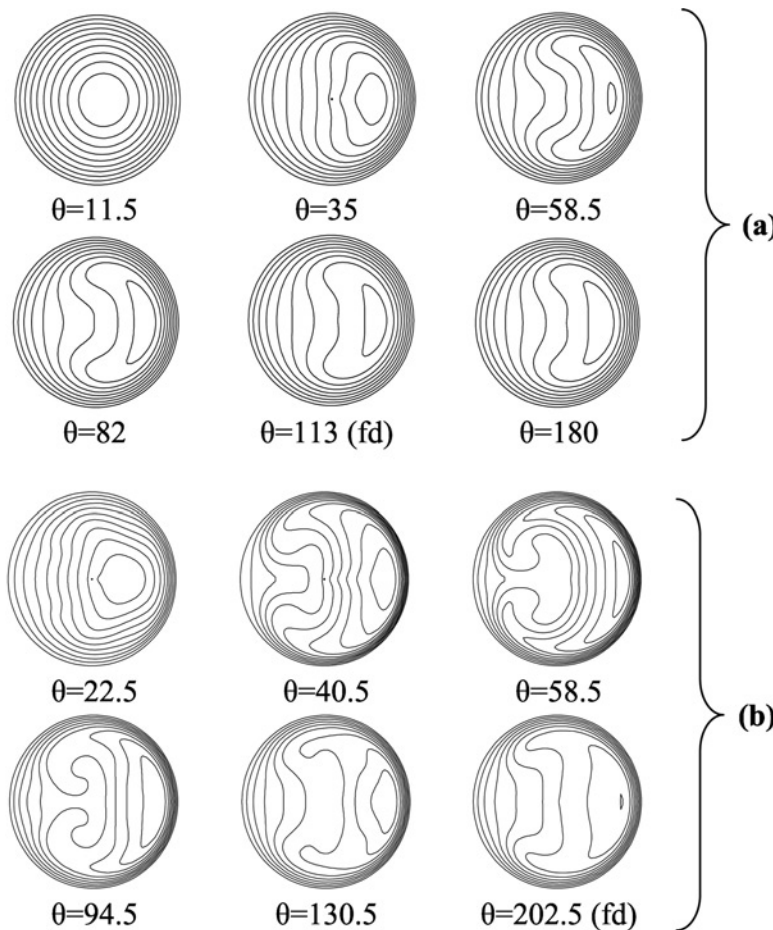


Figure 3.
Grid independency test
for $Dean = 129.4$
($\delta = 1/7, Re = 242$)

Notes: (a) Non-dimensional axial velocity profiles on the section B-B. (b) average friction factor and average Nusselt number along the pipe

1,652. For the higher Dean numbers beyond the specified range, numerical instabilities appear, which is the convergency limitation of the numerical scheme used here. Five different curvature ratios ($\delta = 1/2, 1/3, 1/7, 1/20, 1/30$) are considered to cover both ranges of loose and non-loose curved pipes, and for the thermal analysis two Prandtl numbers of 0.5 and 1 are taken into account at the both thermal boundaries introduced earlier. The numerical results obtained here concentrate on the detailed investigation of flow and temperature fields at the entrance region by a quantitative analysis of hydrodynamic and thermal entrance lengths which have not been studied precisely at the best of our knowledge.

Figure 4 shows the contours of axial velocity at different cross sections of the curved pipe for two Dean numbers. As it is seen in this figure, along the entrance region the location of maximum axial velocity moves from the center of the curved pipe towards the outer wall due to centrifugal effects. Consequently, the thickness of axial flow boundary layer decreases on the outer wall and increases on the inner wall. As the Dean number increases, the location of maximum axial velocity approaches more



Notes: (a) *Dean* = 129.4 ($\delta = 1/7$, *Re* = 242), (b) *Dean* = 481.1 ($\delta = 1/7$, *Re* = 900)

Figure 4. Contours of axial velocity at different sections

closer to the outer wall due to strengthening centrifugal forces. The criterion of development either hydrodynamically or thermally follows Equations (24) and (25).

Figures 5 and 6 represent secondary flows at different cross sections of the curved pipe for the same cases of Figure 4. The secondary flow boundary layer thickness at all De numbers starts increasing from $\Phi = 0$ to $\Phi = 180$ degrees, and as flow proceeds downstream the intensity of the secondary flow increases first and then decreases while approaching the fully developed region. This increasing and decreasing rate is

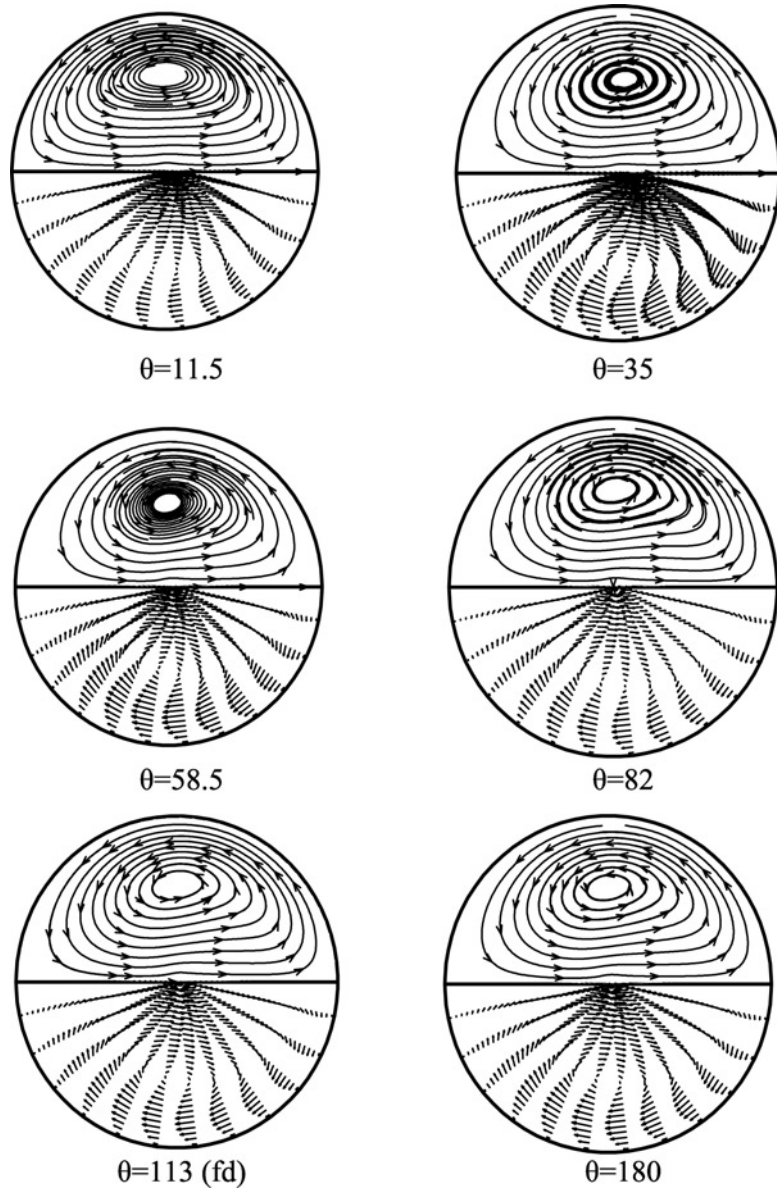
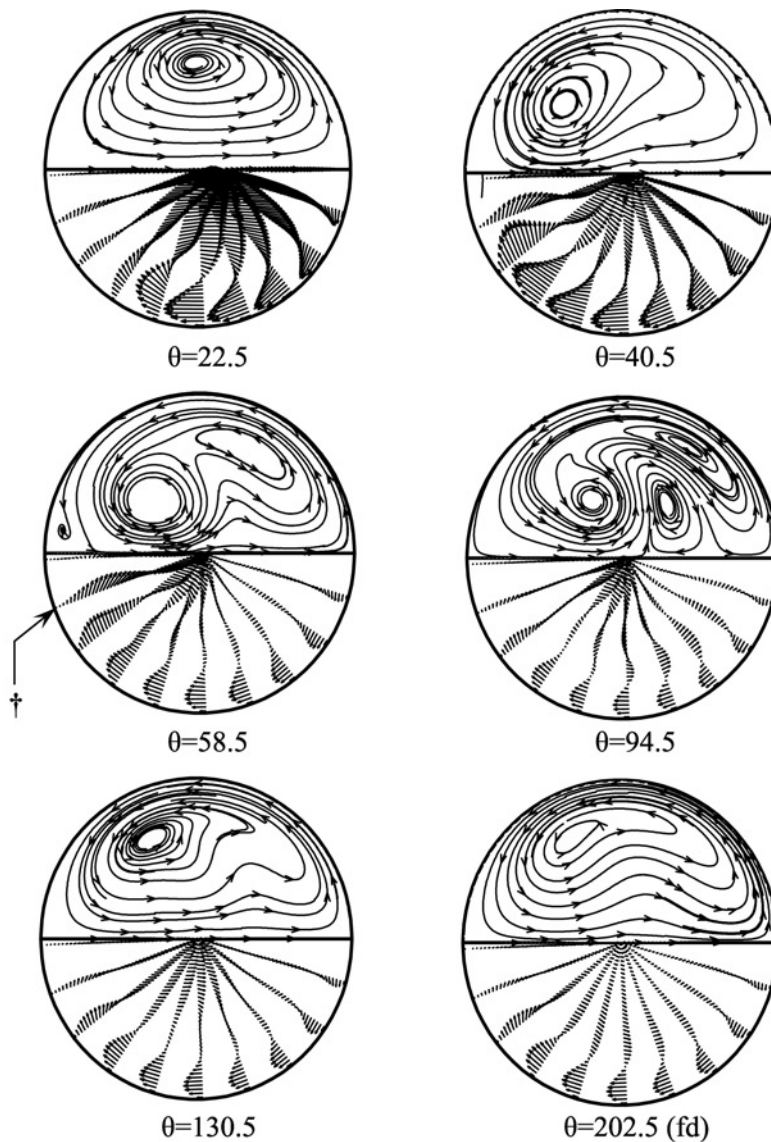


Figure 5.
Streamlines (upper half)
and velocity field of
secondary flow (lower
half) at different sections
for $Dean = 129.4$
($\delta = 1/7, Re = 242$)



Notes: † : s-shaped profile on the wall (separation occurs)

Figure 6. Streamlines (upper half) and velocity field of secondary flow (lower half) at different sections for $Dean = 481.1$ ($\delta = 1/7, Re = 900$)

greater for the high De numbers. For low De numbers (see Figure 5) the secondary flow consists of a pair of counter-rotating cells (one cell is in upper half and the other is in lower half of pipe), called Dean cells. But for higher De numbers due to circumferential adverse pressure gradient, the secondary flow boundary layer becomes s-shaped (see Figure 6). This is due to instability of Dean vortices when De number is greater than the critical value (Mokrani *et al.*, 1997). This instability intensifies until $\theta = 94.5$, leading to another pair of vortices at this section. As the flow proceeds further

downstream, secondary flow boundary layer changes from s-shaped to d-shaped and the Dean vortices disappear, resulting in Dean cells again.

In Figure 7, the development of axial velocity on the symmetry plane and the plane perpendicular to the symmetry plane are shown for the above mentioned two cases. Comparing the axial velocity profiles for the two different Reynolds numbers indicates that the maximum velocity location for large Reynolds number of 900 gets more closer to the outer wall than for low Reynolds number of 242.

Variations of friction factor (C_f) vs circumferential direction (ϕ) at different cross sections of the curved pipe are presented in Figure 8. For low Dean numbers (Figure 8(a)), as the flow proceeds downstream from $\theta = 0$ to 58.5 degrees, the axial velocity gradient has dominant effect on the friction factor which increases at the outer wall ($0 \leq \phi \leq \frac{\pi}{2}$). Beyond approximately $\theta = 58.5$ degrees, friction factor decreases until approaching fully developed region as expected from the strength reduction of secondary flows. However, for high De numbers (Figure 8(b)), the effect of secondary flows becomes more important especially close to the inlet section ($0 < \theta < 40.5$) where the location of maximum friction factor is near high intensity secondary flow region at about $\phi = 45$ (see curve for $\theta = 22.5$) instead of $\phi = 0$ (the location of maximum axial flow gradient). Further downstream, the variation trend of the friction factor for large Dean numbers is almost the same as low one. An important point to be mentioned is that at the inner wall region of the curved pipe ($\frac{\pi}{2} < \phi < \pi$), the axial velocity gradient decreases and the secondary flow strengthens. These two events have opposing effect on friction factor value resulting in smaller variation in the friction factor.

Figure 9 indicates the ratio of average friction factor in a fully developed cross section to this value for straight pipe ($(C_{f,m})_c / (C_{f,m})_s$) vs De number. The comparison of the available semi-empirical data for the loose curved pipes ($\delta > \frac{1}{16}$) with the computed results indicates a very good agreement. Furthermore, for non loose curved

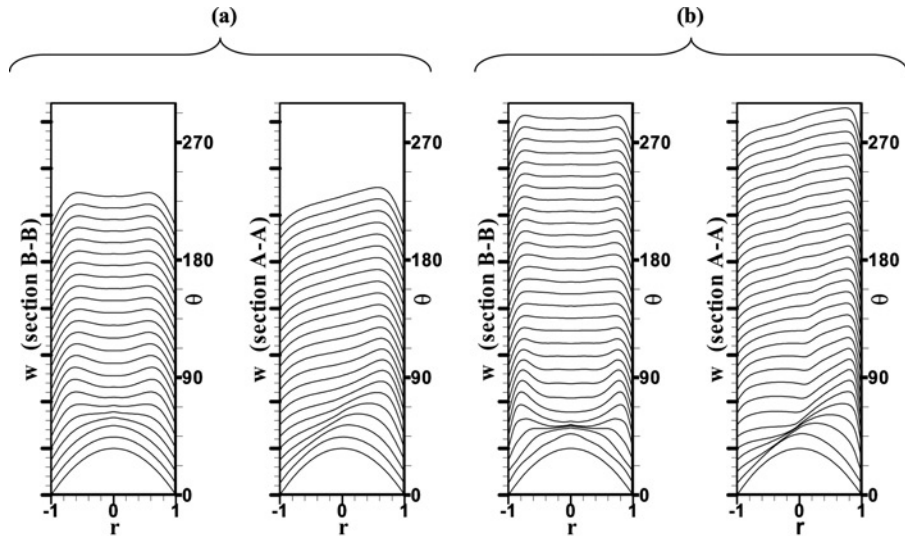
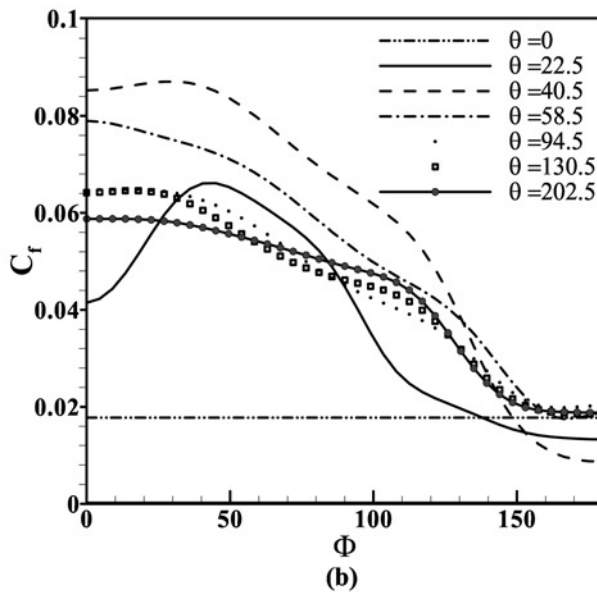
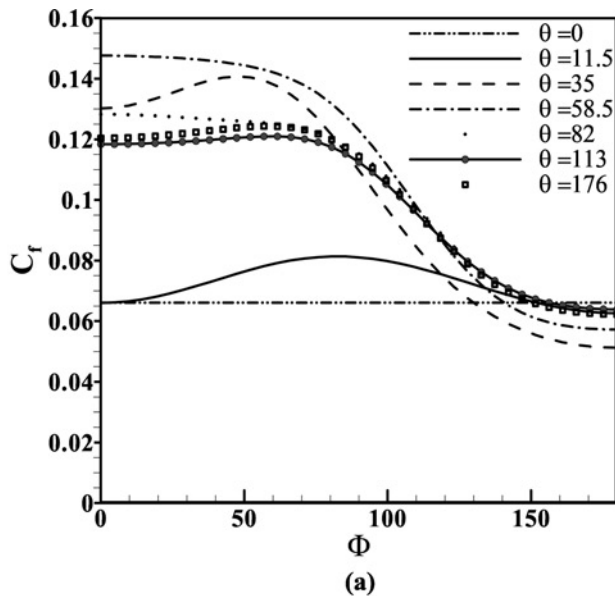


Figure 7.
Development of axial velocity on the section B-B and on the section A-A

Notes: (a) $Dean = 129.4$ ($\delta = 1/7$, $Re = 242$), (b) $Dean = 481.1$ ($\delta = 1/7$, $Re = 900$)



Notes: (a) $Dean = 129.4$ ($\delta = 1/7$, $Re = 242$), (b) $Dean = 481.1$ ($\delta = 1/7$, $Re = 900$)

Figure 8. Friction factor (C_f) vs Φ at different sections

pipes ($\delta < \frac{1}{16}$), the normalized average friction factor vs De number shown in Figure 9 predicts slightly larger values than semi-empirical results (loose curved pipes). This is physically true due to the presence of large velocity gradients in the curved pipes with high curvatures ($\delta < \frac{1}{16}$).

Variations of the cross sectional average friction factor ($C_{f,m}$) along the axial direction of the curved pipe in the entrance region is represented in Figure 10. Figure

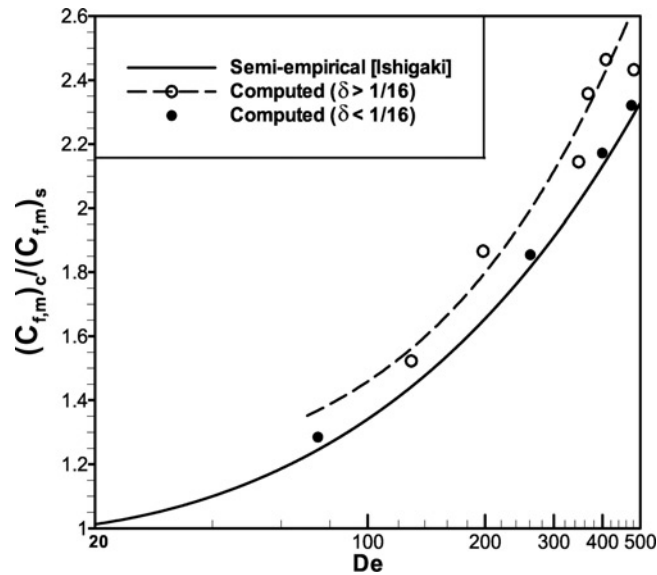


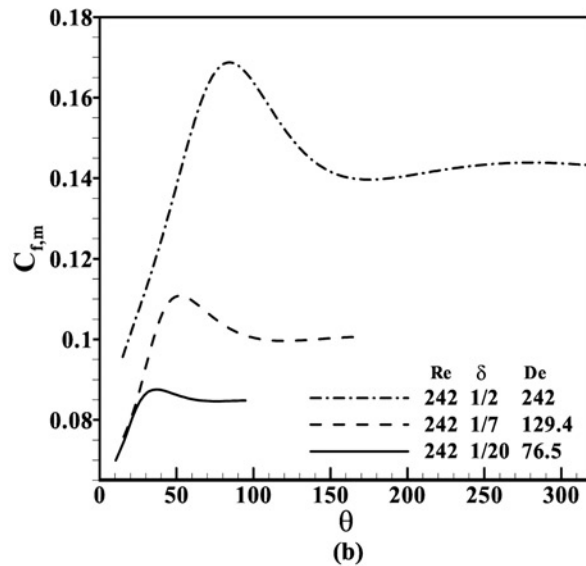
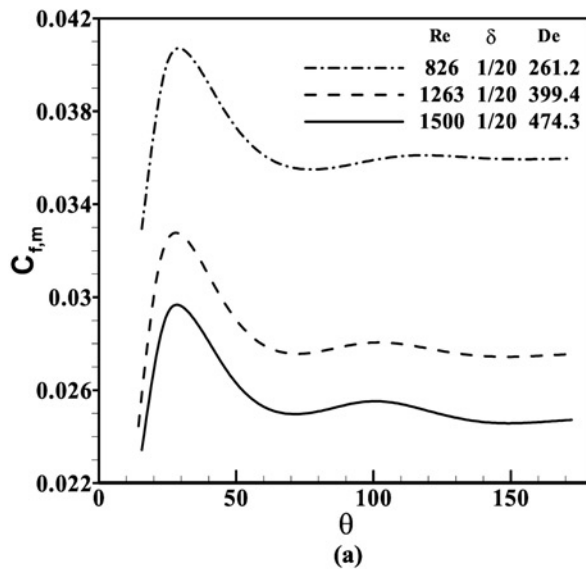
Figure 9.
Normalized friction factor
vs De in fully developed
region

10(a) is for three different Reynolds numbers and a fixed curvature, and Figure 10(b) is for three different curvatures at a fixed Reynolds number. As discussed earlier (Figure 8) the friction factor has a maximum value in the entrance region which decreases to the fully developed constant value at all cases. In this figure, the cyclic behavior of friction factor due to Dean instability which is stronger for high De numbers is observed in the entrance region of curved pipes.

To investigate the dependence of the hydrodynamic and thermal entrance length on the Reynolds number and curvature ratio in curved pipes, Figures 11(a) and (b) are represented. As it is clear from the numerical results, for small curvature ratios (less than $\frac{1}{7}$), the hydrodynamic entrance lengths increase as curvature ratios decrease. For larger curvature ratios (greater than $\frac{1}{7}$) the entrance lengths depend only on the Reynolds number. Similar trend can be observed for the thermal entrance lengths. Since, curvature ratio has small effect on the entrance length except in the very small curvature ratios, De as a function of Re and δ is not a pertinent parameter in entrance length considerations.

For the thermal analysis in the entrance region of the curved pipe, consider Figures 12 and 13 which indicate temperature contours at different cross sections along the entrance region for different thermal boundary conditions with I.B.2 inlet profile. It can be seen that within the whole entrance region, the trend of temperature field variations is similar to the axial velocity field (Figure 4) which is also shown by Ishigaki (1999) in fully developed region. Another point is that developing of temperature profile for constant heat flux goes on further down stream than of constant temperature at the wall, resulting in longer thermal entrance length in constant heat flux case. At high De numbers (Figure 13), the temperature field is affected by strong secondary flows and becomes corrugated near the curved pipe inlet due to Dean instabilities.

The local Nusselt number vs circumferential direction at different cross sections is shown in Figure 14. Due to high temperature gradients at the outer wall, the local



Notes: (a) $\delta = 1/20$ and $Re = (826, 1263, 1,500)$, (b) $Re = 242$ and $\delta = (1/2, 1/7, 1/20)$

Figure 10. Average friction factor ($C_{f,m}$) vs θ

Nusselt number becomes maximum at that region. In Figure 15, the cross sectional average Nusselt number vs axial direction for two De numbers and two thermal boundary conditions at the inlet in the case of constant temperature at the wall is shown. Reduction of temperature gradient from infinity for case I.B.1 causes the average Nusselt number (Nu_m) to decrease near the inlet. When flow moves further downstream, for both cases I.B.1 and I.B.2, Nu_m in the entrance region fluctuates because of Dean instabilities. The fluctuation gets stronger as Dean number increases.

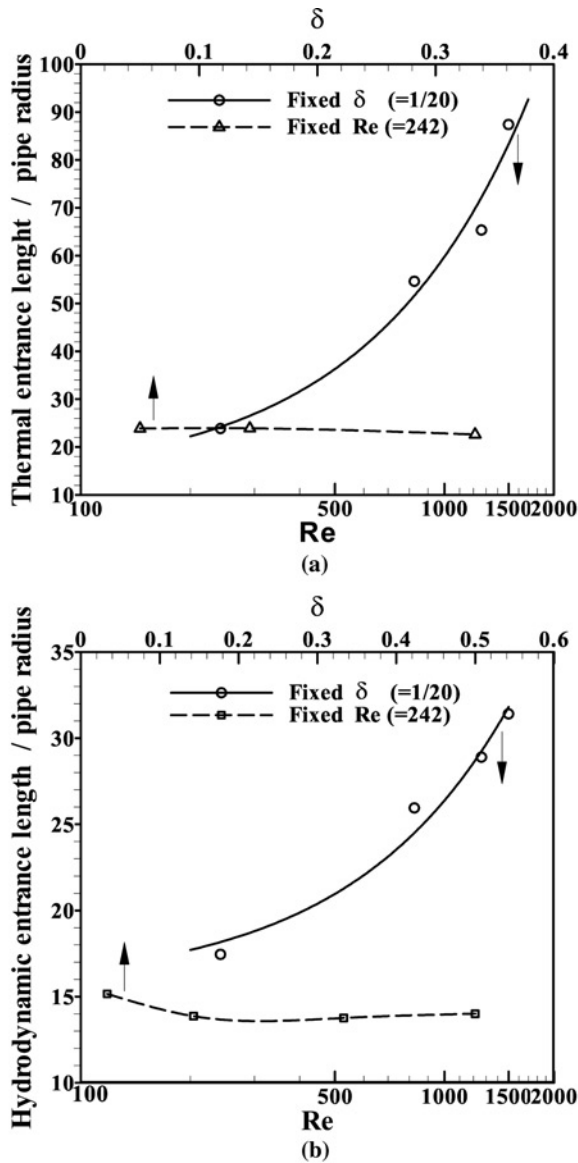
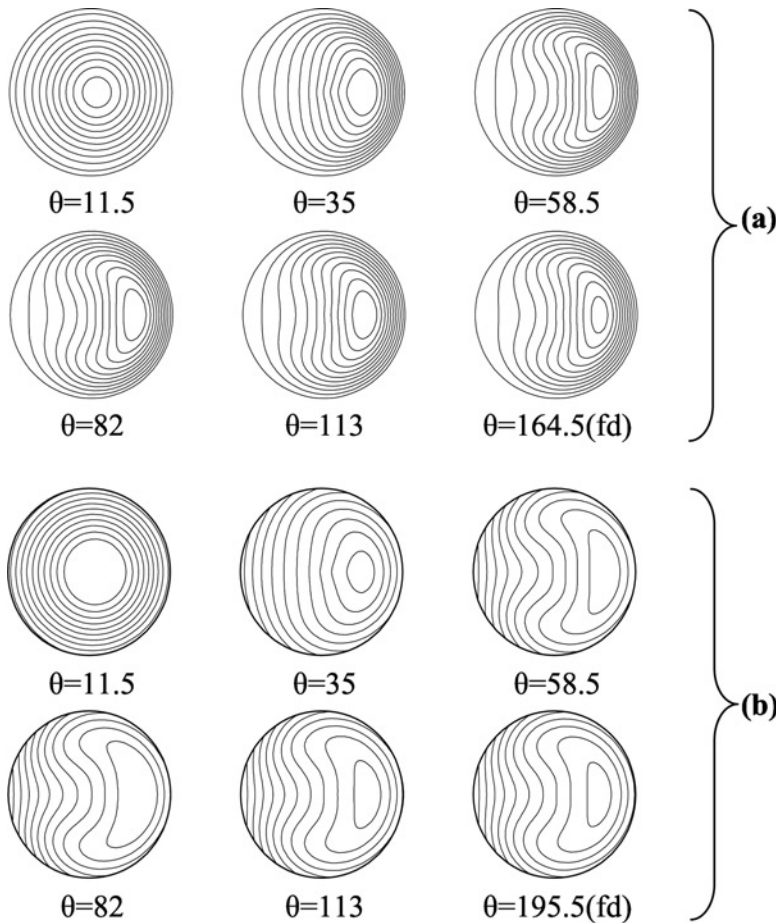


Figure 11.
Hydrodynamic and
thermal entrance length

Notes: (a) Hydrodynamic entrance length vs δ for $Re = 242$ and vs Re for $\delta=1/20$, (b) Thermal entrance length (for constant heat flux at the wall and $Pr = 0.5$) vs δ for $Re = 242$ and vs Re for $\delta=1/20$

Figure 16 indicates variations of cross sectional average Nusselt number against axial direction of the curved pipe for two De numbers at two inlet thermal boundary conditions in the case of constant heat flux. As it can be observed from these figures, the fully developed Nusselt number is independent of inlet profiles and two results coincide each other. In case of I.B.2 which is for thermally fully developed condition of a straight pipe, the inlet Nusselt number (at $\theta = 0$) obtained from numerical results is



Notes: For I. B. 2, $Dean = 129.4$ ($\delta = 1/7$, $Re = 242$) and $Pr = 0.5$.
 (a) $T_s = \text{const}$, (b) $q_s = \text{const}$

Flow and heat transfer in a curved pipe

Figure 12. Contours of temperature at different sections

the same as analytical value of $\frac{3.66}{2}$ for constant wall temperature (Figure 15) and $\frac{4.36}{2}$ for constant heat flux (Figure 16). In these figures, the oscillations of Nusselt number due to Dean instability (stronger for high De numbers) is observed in entrance region. The oscillating strength of secondary flow along entrance region as explained in Figures 5 and 6 lead to this oscillating behavior of Nusselt number. In addition to high De numbers, in the case of constant heat flux, the inlet temperature profile also affects the oscillations in such a way that uniform inlet (I.B.1) tends to more severe oscillations than fully developed one (I.B.2).

The logarithmic trend of bulk temperature for constant wall temperature (Figure 15) and linear trend of bulk temperature for constant heat flux conditions at the wall (Figure 16) in the curved pipe are similar to the straight one. Also, in Figure 16 the temperature values at three different points of the wall including $\Phi = 0, 90$ and 180

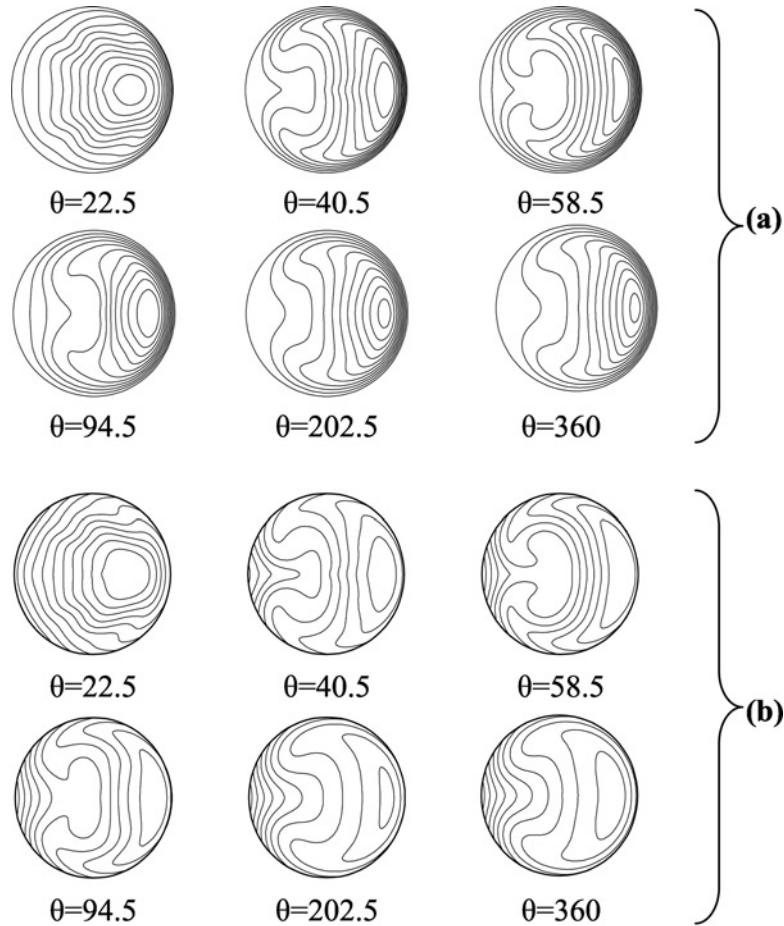


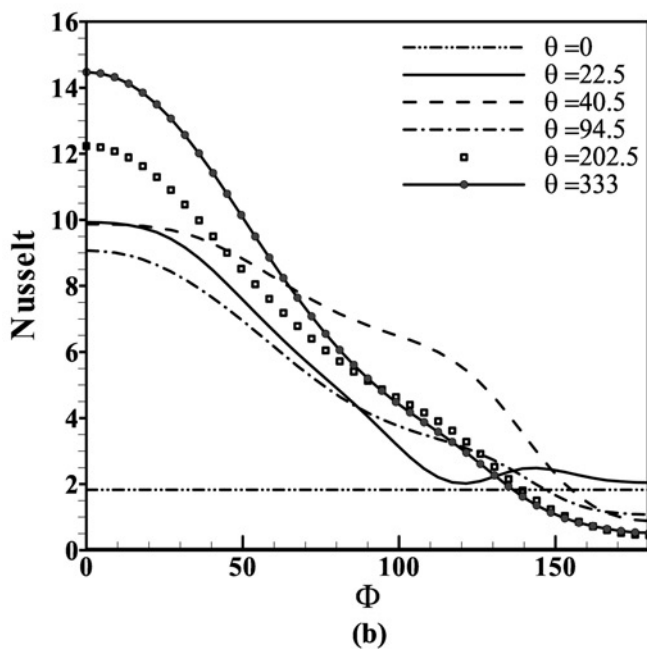
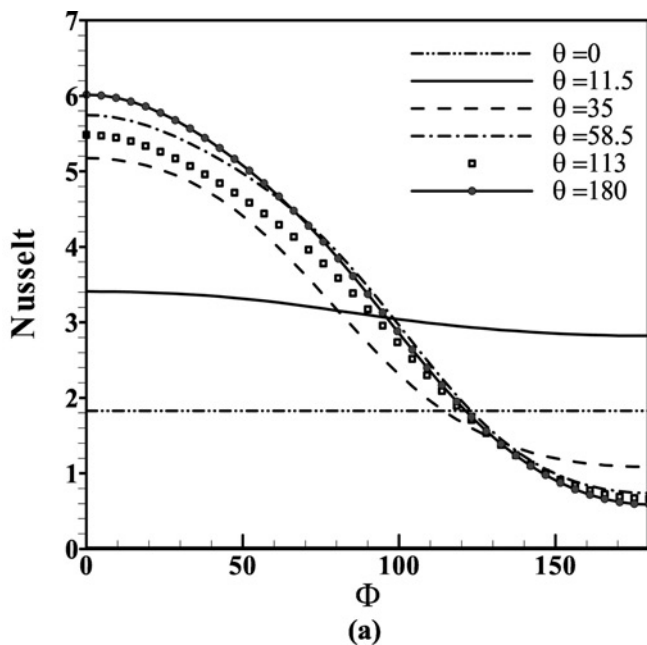
Figure 13.
Contours of temperature
at different sections

Notes: For I. B. 2, $Dean = 481.1$ ($\delta = 1/7$, $Re = 900$) and $Pr = 0.5$.
(a) $T_s = \text{const}$, (b) $q_s = \text{const}$

degrees along the axial direction of the curved pipe are shown, where the maximum temperature belongs to the inner wall due to low convection effect on that location.

For another verification in fully developed region, the normalized average Nusselt number for the curved pipe (the ratio of average Nusselt number at a fully developed section for the curved pipe to this value for straight pipe) is compared with the semi-empirical data (Figure 17) presented by Ishigaki (1996, 1994), which is valid in the range of $\delta < \frac{1}{16}$.

Finally, in Figure 18, the average Nusselt number overall the entrance region of curved pipe vs De is presented at different thermal boundary conditions for case I.B.1. This quantity is a criterion of average heat transfer rate per unit area of the pipe in entrance region. The results indicate that the Nusselt number increases as Dean number increases, which is achieved with increase of either Reynolds number or



Notes: For I. B. 2, (in the case of $T_s = \text{const}$) and $Pr = 0.5$. (a) $Dean = 129.4$ ($\delta = 1/7, Re = 242$), (b) $Dean = 481.1$ ($\delta = 1/7, Re = 900$)

Figure 14.
Local Nusselt number vs Φ at different sections for

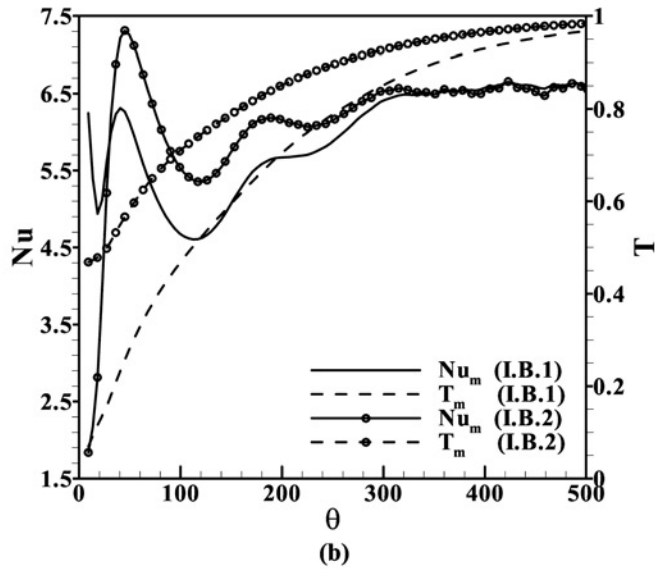
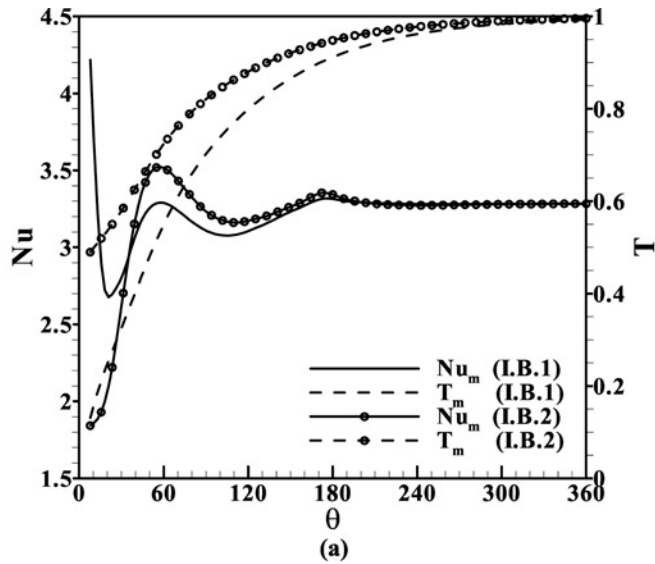
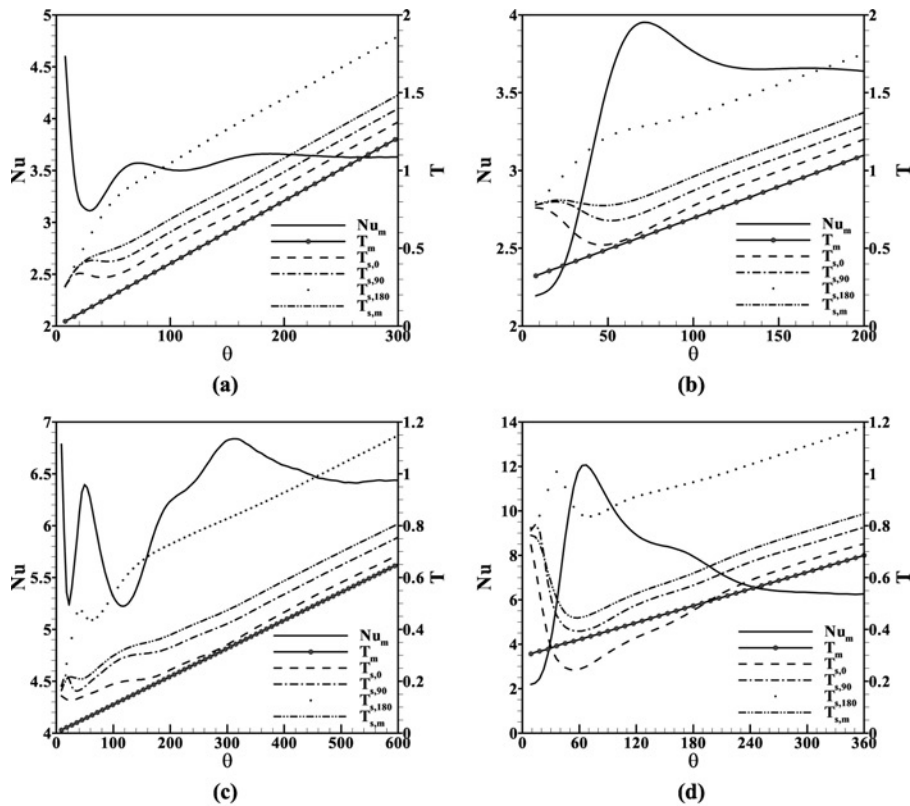


Figure 15.
Average Nusselt number
(\overline{Nu}_m) vs θ

Notes: For $T_s = \text{const}$ and $Pr = 0.5$. (a) $Dean = 129.4$ ($\delta = 1/7$, $Re = 242$),
(b) $Dean = 481.1$ ($\delta = 1/7$, $Re = 900$)

curvature of the pipe. Furthermore, average heat transfer rate in the entrance region for the constant heat flux case at the wall is larger than the constant temperature case at the wall. Also, with the increase of Pr number from 0.5 to 1, heat transfer rate enhances about 27 percent in constant temperature case and 22 percent in constant heat flux case within the entrance region.



Notes: For $q_s = \text{const}$ and $Pr = 0.5$. (a) $Dean = 129.4$ ($\delta = 1/7$, $Re = 242$), I. B. 1, (b) $Dean = 129.4$ ($\delta = 1/7$, $Re = 242$), I. B. 2, (c) $Dean = 481.1$ ($\delta = 1/7$, $Re = 900$), I. B. 1, and (d) $Dean = 481.1$ ($\delta = 1/7$, $Re = 900$), I. B. 2

Figure 16.
Average Nusselt number
(Nu_m) vs θ

5. Conclusion

In this article, developing flow and heat transfer in a curved pipe are studied numerically by solving full Navier-Stokes and energy equations employing the projection method based on second order finite difference discretization at different thermal boundaries and inlet conditions. The outcome of numerical results can be summarized as follows.

The intensity of secondary flow increases near the inlet and then decreases, especially in the case of high Dean numbers due to formation of Dean vortices. This causes friction factor decreases from a maximum value within the entrance region until approaching the fully developed region. Therefore, regardless of inlet profiles, maximum friction factor and also maximum heat transfer rate occurs in the entrance region.

When loose coil approximation is not valid ($\delta > \frac{1}{16}$), the results predict larger values for normalized mean friction factor at fully developed region than the values predicted by semi-empirical curves obtained for loose curved pipes (Ishigaki, 1994, 1996). Because of more intensity of secondary flows, the friction factor in non-loose curved pipes is greater than that of the loose ones.

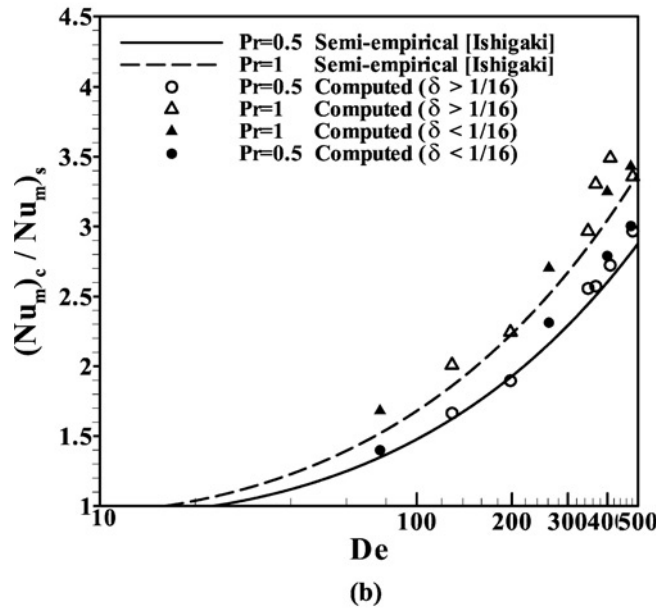
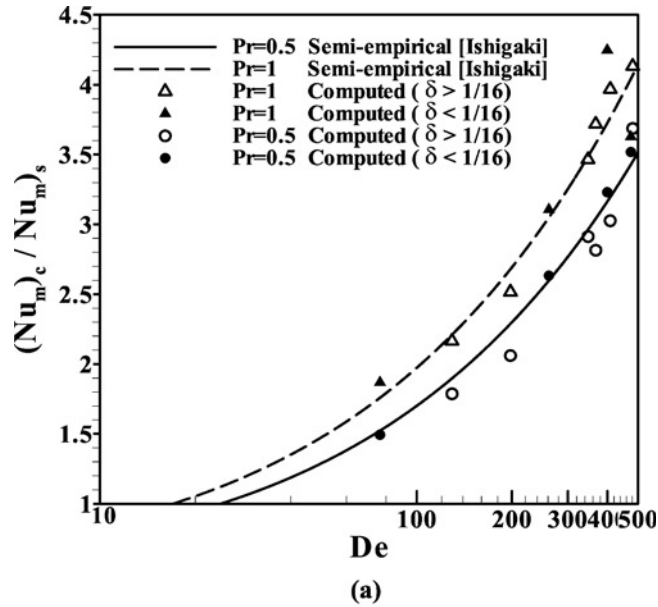


Figure 17.
Average Nusselt number
(Nu_m) vs De in fully
developed region

Notes: (a) $T_s = \text{const}$, (b) $q_s = \text{const}$

Within the entrance region the maximum velocity location shifts from the center to the outer wall of the curved pipe. As Reynolds number increases maximum axial velocity location gets more closer to the outer wall.

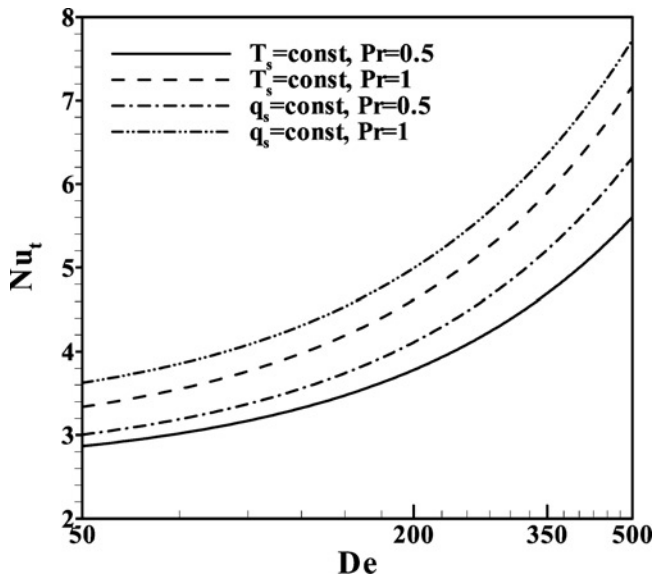


Figure 18. Total Nusselt number for the curved pipe (Nu_t) vs De for I.B.1

The entrance length dependence on curvature ratio is just considerable for curvature ratios less than $\frac{1}{7}$ and is negligible beyond this value. Therefore, Dean number is not a pertinent parameter and the entrance length depends only on Reynolds number especially for $\delta > \frac{1}{7}$.

References

- Acharya, N., Sen, M. and Chang, H.C. (1993), "Thermal entrance length and Nusselt numbers in coiled tubes", *International Journal of Heat and Mass Transfer*, Vol. 37, pp. 336-40.
- Adler, V.M. (1934), "Strömung in gekrümmten Rohren", *Zeitschrift für Angewandte Mathematik und Mechanik*, Vol. 14, pp. 257-75.
- Anderson, J.D. (1995), *Computational Fluid Dynamics: The Basics with Applications*, Ch. 4, MGH, New York, NY.
- Austin, L. (1971), "The development of viscous flow within helical coils", PhD thesis, University of Utah, Salt Lake City, UT.
- Bara, B., Nandakumar, K. and Masliyah, J.H. (1992), "An experimental and numerical study of the Dean problem: Flow development towards two-dimensional multiple solution", *Journal of Fluid Mechanics*, Vol. 244, pp. 339-76.
- Bejan, A. (1984), *Convection Heat Transfer*, Ch. 3, Wiley, New York, NY.
- Berger, B.A., Talbot, L. and Yao, L.S. (1983), "Flow in curved pipes", *Annual Review of Fluid Mechanics*, Vol. 15, pp. 461-512.
- Chorin, J.A. (1968), "Numerical solution of the Navier-Stokes equations", *Mathematics and Computing*, Vol. 22 No. 104, pp. 745-62.
- Collins, W.M. and Dennis, S.C.R. (1975), "The steady motion of a viscous fluid in a curved tube", *Quarterly Journal of Mechanics and Applied Mathematics*, Vol. 28, pp. 133-56.
- Comini, G., Croce, G. and Nonino, C. (2004), "Modeling of convection enhancement mechanisms", *International Journal of Numerical Methods for Heat and Fluid Flow*, Vol. 14 No. 1, pp. 66-84.

- Dean, W.R. (1927), "Note on the motion of fluid in a curved pipe", *Philosophical Magazine*, Vol. 20, pp. 208-23.
- Dean, W.R. (1928), "The streamline motion of fluid in a curved pipe", *Philosophical Magazine*, Vol. 30, pp. 673-95.
- Humphrey, J.A.C. (1977), "Flow in ducts with curvature and roughness", PhD thesis, Imperial College of Science and Technology.
- Ishigaki, H. (1994), "Analogy between laminar flows in curved pipes and orthogonally rotating pipes", *Journal of Fluid Mechanics*, Vol. 268, pp. 133-45.
- Ishigaki, H. (1996), "Laminar flow in rotating curved pipes", *Journal of Fluid Mechanics*, Vol. 329, pp. 373-88.
- Ishigaki, H. (1999), "Analogy of forced convective heat transfer between laminar flows in curved pipes and orthogonally rotating pipes", *JSME International Journal Series B*, Vol. 42 No. 1, pp. 48-55.
- Ito, H. and Nanbu, K. (1971), "Flow in rotating straight pipes of circular cross section", *ASME Journal of Basic Engineering*, Vol. 93, pp. 383-94.
- Kumar, V. and Nigam, K.D.P. (2005), "Numerical simulation of steady flow fields in coiled flow inverter", *International Journal of Heat and Mass Transfer*, Vol. 48, pp. 4811-28.
- Le Guer, Y., Castelain, C. and Peerhossaini, H. (2001), "Experimental study of chaotic advection regime in a twisted duct flow", *European Journal of Mechanics B – Fluids*, Vol. 20, pp. 205-32.
- Lee, G.H. and Baek, J.H. (2002), "A numerical study on the similarity of fully developed turbulent flows between in orthogonally rotating square ducts and stationary curved square ducts", *International Journal of Numerical Methods for Heat and Fluid Flow*, Vol. 12, pp. 241-57.
- Lee, G.H. and Baek, J.H. (2006), "Effect of aspect ratio on the similarity between developing laminar flows in orthogonally rotating ducts and stationary curved ducts", *International Journal of Numerical Methods for Heat and Fluid Flow*, Vol. 16 No. 4, pp. 494-508.
- Mokrani, A., Castelain, C. and Peerhossaini, H. (1997), "The effects of chaotic advection on heat transfer", *International Journal of Heat and Mass Transfer*, Vol. 40 No. 13, pp. 3089-104.
- Nobari, M.R.H. and Gharali, K. (2006), "A numerical study of flow and heat transfer in internally finned rotating straight pipes and stationary curved pipes", *International Journal of Heat and Mass Transfer*, Vol. 49, pp. 1185-94.
- Nonino, C. and Comini, G. (2002), "Convective heat transfer in ribbed square channels", *International Journal of Numerical Methods for Heat and Fluid Flow*, Vol. 12 No. 5, pp. 610-28.
- Papa, F., Keith, T.G. Jr., DeWitt, K.J. and Vaidyanathan, K. (2002), "Numerical calculation of developing laminar flow in rotating ducts with a 180 bend", *International Journal of Numerical Methods for Heat and Fluid Flow*, Vol. 12 No. 7, pp. 780-99.
- Patankar, S.V., Pratap, V.S. and Spalding, D.B. (1974), "Prediction of laminar flow and heat transfer in helically coiled pipes", *Journal of Fluid Mechanics*, Vol. 62, pp. 539-51.
- Shah, R.K. and Joshi, S.D. (1987), "Convective heat transfer in curved ducts", in Kakac, S., Shah, R.K. and Aung, W. (Eds), *Handbook of Single-Phase Convective Heat Transfer*, Ch. 5, Wiley, New York, NY.
- Soh, W.Y. and Berger, S.A. (1984), "Laminar entrance flow in a curved pipe", *Journal Fluid Mechanics*, Vol. 148, pp. 109-35.
- Temam, R. (1978), "Navier-Stokes Equations", North-Holland, Amsterdam.
- Trefethen, L.M. (1957), "Flow in rotating radial ducts", *Report No. 55GL350-A*, General Electric Company, Fairfield, CT.

Williams, G.S., Hubbell, C.W. and Fenkell, G.H. (1902), "Experiments at Detroit, Mich., on the effect of curvature upon the flow of water in pipes", *Transactions of ASCE*, Vol. 47, pp. 1-196.

Zheng, B., Lin, C.X. and Ebadian, M.A. (2000), "Combined laminar forced convection and thermal radiation in a helical pipe", *International Journal of Heat and Mass Transfer*, Vol. 43, pp. 1067-78.

Further reading

Li, L.J., Lin, C.X. and Ebadian, M.A. (1998), "Turbulent mixed convective heat transfer in the entrance region of a curved pipe with uniform wall-temperature", *International Journal of Heat and Mass Transfer*, Vol. 41, pp. 3793-805.

Corresponding author

M.R.H. Nobari can be contacted at: mrnobari@cic.aut.ac.ir